Unified Mie and fractal scattering by biological cells and subcellular structures

Tao T. Wu,[1,*] Jianan Y. Qu,[1] and Min Xu[2]

[1]*Department of Electronic and Computer Engineering, Hong Kong University of Science and Technology, Hong Kong, China*

[2]*Department of Physics, Fairfield University, Fairfield, Connecticut 06824, USA*

[*]*Corresponding author: eewt@ust.hk*

Received April 17, 2007; revised June 8, 2007; accepted June 20, 2007; posted June 26, 2007 (Doc. ID 82189); published August 2, 2007

Angle-resolved light scattering spectroscopy of biological cells is investigated in the visible wavelength range. A unified Mie and fractal model is shown to provide an accurate global agreement with light scattering spectra from 1.1° to 165° scattering angles. It is found that light scattering in forward directions (<8°) is dominated by Mie scattering by the bare cell and nucleus, whereas light scattering at large angles (>20°) is determined by fractal scattering by subcellular structures. The findings are consistent with the results of experimental investigation of the contributions of different cellular components to light scattering by cells. © 2007 Optical Society of America

OCIS codes: 290.0290, 290.4020, 120.5820, 170.1530.

An understanding of the relationship between light scattering by cells and cellular structures is essential for noninvasive optical diagnostics based on the measurement of light scattering signals from biological samples. Light scattering spectroscopy is an important tool for studying the structural features of cells and tissue [1–4]. Mie scattering is frequently used to interpret cell light scattering signals [1–5]. However, such a model is not adequate to provide a satisfactory description of the optical signal at large scattering angles owing to the dominance of light scattering from small subcellular structures that exhibit a fractal nature [3,4]. The simulation of cell scattering via computational solutions of Maxwell's equations with the finite-difference time-domain (FDTD) method indicated that the large-angle scattering signals would be significantly affected by the fluctuation of the refractive index and the shape of small-sized scatterers in cells [6,7]. Though with detailed information on cellular structures FDTD simulation can potentially provide a thorough description of cell light scattering, it is computationally time consuming. It is desirable to develop a simple and analytical model for light scattering by biological cells that takes into account scattering from both bare cells and intracellular components.

This study aims to understand and quantify light scattering by bare cells and intracellular structures. A unified Mie and fractal model is developed to interpret light scattering from biological cells. Here, the cell is treated as an optically soft complex particle. The unified model based on a superposition rule provides a simple means to analyze light scattering by a biological cell and to quantify the contributions from each individual inclusion [8]. Specifically, the bare cell and nucleus are modeled as spheres with a uniform index of refraction. Their scattering is described by Mie scattering. The subcellular structures are modeled as a fractal continuous random medium. Light scattering caused by weak random fluctuations of the dielectric permittivity is computed with a fractal model [9,10]. In this Letter, we show that Mie scattering from the bare cell and the nucleus dominates cell light scattering in the forward directions. Fractal scattering caused by random fluctuation of the background refractive index within the cell (and nucleus) dominates light scattering by cells in larger angles. The unified model is validated by experimental angle-resolved light scattering spectra of SiHa epithelial cell samples.

By treating light scattering from one biological cell as from a complex soft particle comprising the bare cell, the nucleus, and random fluctuations of the background refractive index within the cell, the superposition rule [8] showed that the squared scattering amplitude function, describing light scattered into direction θ at wavelength λ, can be approximated by [8]

$$\overline{|S_{Cell}(\lambda,\theta)|^2} = |S_0(\lambda,\theta)|^2 + |S_n(\lambda,\theta)|^2 + |S_{bg}(\lambda,\theta)|^2 \tag{1}$$

after configurational averaging over all possible sizes, shapes, and orientations of the cell and the relative position of its inclusions. Here $|S_0(\lambda,\theta)|^2$ and $|S_n(\lambda,\theta)|^2$ are the squared scattering amplitude functions for the bare cell and the nucleus, respectively, and can be modeled by Mie scattering of homogeneous spheres. $|S_{bg}(\lambda,\theta)|^2$ is the fractal scattering term given by [10]

$$|S_{bg}(\lambda,\theta)|^2 = \beta^2 \int_0^{(2\pi n_0/\lambda) l_{max}} \frac{(2\pi n_0/\lambda)^{D_f-1} x^{6-D_f}}{[1+2(1-\cos\theta)x^2]^2} \mathrm{d}x. \tag{2}$$

The strength of fractal light scattering depends on the fractal dimension D_f and the refractive index fluctuation strength $\beta \propto n_0 \Delta n$, as well as the cutoff correlation length l_{max}, where n_0 and Δn are the mean refractive index of the biological cell and the fluctuation amplitude of refractive index, respectively.

To validate the unified model of light scattering by cells, we measured the wavelength- and angular-dependent light scattering signals from the SiHa epithelial cells in phosphate buffered saline (PBS) suspensions and monolayer cultures, respectively. However, we focused our study on the scattering from the cell suspension, where the bare cell and nucleus could be considered spherical Mie scatterers. It is known that acetic acid can induce transient changes of the refractive indices of subcellular structures that contribute to acetowhitening, the effect that colposcopic diagnosis of precervical cancer is based on [11]. Acetic acid was used to modulate the scattering properties of cell samples. We measured the scattering spectra of cell samples before and after the application of acetic acid.

The details of the light scattering spectroscopy system and sample preparations were described in [12]. The scattering spectra were measured in the angle range from 1.1° to 165° and in the wavelength range from 400 to 700 nm, respectively. The size distribution of the cells in suspension was measured by phase contrast microscopy and verified by a Multisizer II Coulter counter [4]. The size distribution of nuclei was measured by fluorescence microscopy. The nuclei were stained with Hoechst 33342 for fluorescence microscopic imaging. Here, the size distributions of SiHa cells and nuclei were described by log-normal distributions [4]. Specifically, the diameters of the cells in suspension before and after the application of acetic acid were $\phi = 13.80 \pm 1.60$ and $\phi' = 14.40 \pm 1.80$ μm, respectively. The diameters of nuclei before and after the application of acetic acid were $\psi = 9.80 \pm 1.80$ and $\psi' = 9.30 \pm 1.60$ μm, respectively. These size distributions were used in fitting the scattering spectral data.

In the fitting analysis, the mean refractive indices of bare cells and nuclei were assumed to be constant over the wavelength range from 400 to 700 nm. The refractive index of the PBS and the acetic acid solution was assumed to be 1.334. S_0 and S_n in Eq. (1) were computed by using the MIEV0 code [13]. The fitting parameters were refractive indices of cells and nuclei, n_{Cell} and $n_{Nucleus}$, the fractal dimension D_f, the refractive index fluctuation strength β, and cutoff correlation length l_{max}. To obtain the initial values of fitting parameters for Mie scattering, we fitted the scattering spectra in the angle range smaller than 5° by using S_0 and S_n in Eq. (1) because the scattering in this angle range is determined mainly by the Mie scattering of the bare cell and nucleus [7]. We fitted the scattering spectra in the angle greater than 20° [7] by using Eq. (2) to determine the initial fitting parameters of the fractal model. The global fitting of the experimental spectral data over the whole wavelength and angle range was then conducted by minimizing the χ^2 error of all fittings by using the Levenberg–Marquardt optimization.

Typical fitting results of light scattering from the cell suspensions before and after the application of acetic acid are shown in Fig. 1. As can be seen, the unified Mie and fractal model produced accurate fitting of the scattering spectra at all 44 measured

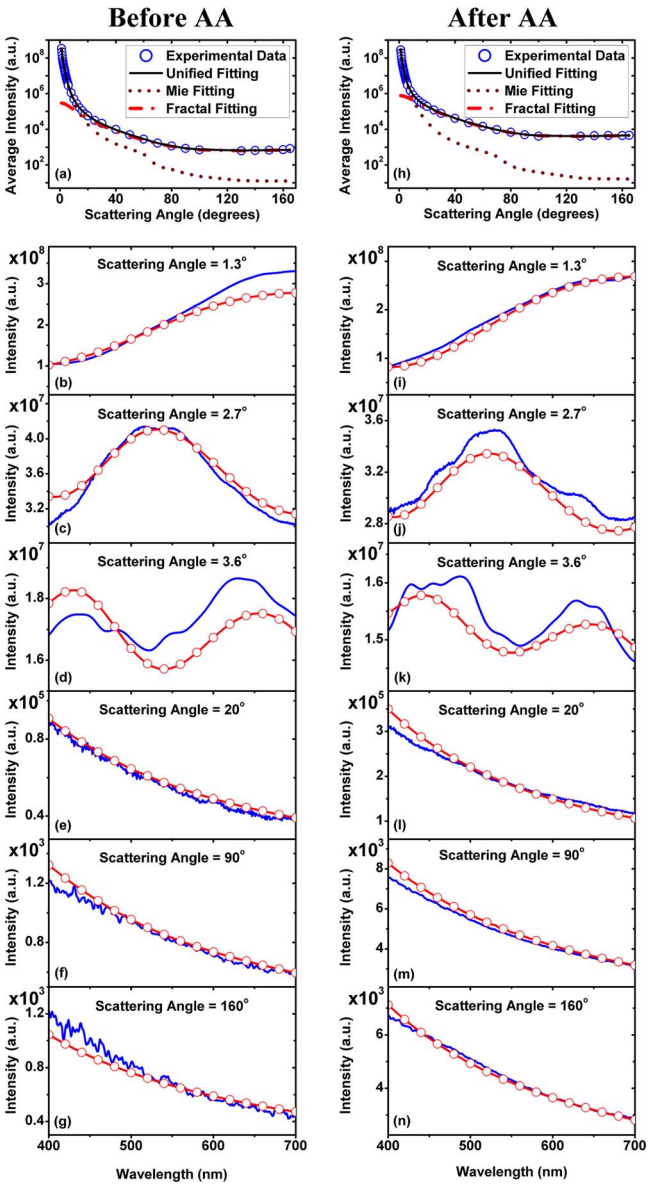

Fig. 1. (Color online) Experimental and fitting results from the measurements before the application of acetic acid: (a) angular-dependent light scattering signals (averaged intensity from 400 to 700 nm); (b)–(g) light scattering spectra at representative angles. After the application of acetic acid: (h) angular-dependent light scattering signals; (i)–(n) light scattering spectra at representative angles. Solid curves, experimental spectra; curves with circles, fitting spectra.

angles. It should be emphasized that the results were obtained by a global fitting based on a single set of fitting parameters. The angular fittings shown in Figs. 1(a) and 1(h) indicate that the Mie scattering from the bare cell and nucleus dominates the scattering spectra in the forward angles (<8°), while the scattering in the large angles (>20°) is determined by fractal scattering from subcellular structures of size less than half a micronmeter. In the angle range from 8° to 20°, the contributions from Mie scattering and fractal scattering are comparable. The results are consistent with the FDTD study of Brock *et al.* [7]. The detailed fittings of scattering spectra at representative angles are shown in Figs. 1(b)–1(g) and

1(i)–1(n). The typical oscillation pattern of Mie scattering appears in the scattering spectra at small angles, while the fractal scattering decays monotonically as a function of wavelength.

The fitting parameters are listed in Table 1, where Δn_1 and Δn_2 are the fluctuation amplitudes of the refractive index before and after the application of acetic acid, respectively. After the application of acetic acid the mean refractive index of the cell decreases slightly because of the increase of the cell size. This is consistent with previously reported swelling of cells induced by acetic acid [14]. In contrast, the mean refractive index of the nuclei increases slightly, probably beacause of the shrinkage of the nuclei size induced by acetic acid. The slight increase of fractal dimension, D_f, after the application of acetic acid indicates an increase of volume fraction of the small-sized subcellular structures. One remarkable finding is that acetic acid induced a significant increase of the β value. The ratio of β values before and after the application of acetic acid reflects the ratio of fluctuation amplitudes of the refractive index in cell. The fractal scattering contribution to large-angle scattering signals increases by a factor of 5–9 due to both the increase of the fluctuation amplitude of the refractive index by a factor of 1.81 and the increase of the volume fraction of the small-sized subcellular structure after the application of acetic acid. This is consistent with the experimental results that small-sized organelles in cytoplasm are the major contributors to the increase of large-angle scattering induced by acetic acid [12]. Along with the intensity increase in the large scattering angles, the anisotropy factor g for the cell is reduced, accompanied by a decrease in the cutoff correlation length l_{max} [10]. The fractal component of light scattering by cells in a large angle is not sensitive to l_{max}. Finally, this analysis confirms the hypothesis of the acetowhitening effect, that acetic acid increases the polymerization of cytokeratins and causes the self-organization of keratin filaments into larger bundles [15].

To further validate the fractal nature of scattering in large angles, we analyzed the angle-resolved scattering spectra of monolayer cell cultures. The shapes of cells and nuclei are irregular in monolayers because cells spread over the culture dish. The model of spherical Mie scatterers is not applicable to light scattering by cell and nucleus in forward directions. We used the fractal model to fit the scattering spectra in scattering angles larger than 20°. Accurate global fitting was achieved for the spectral data measured both before and after the application of acetic acid. All the scattering spectra in the large angles decay monotonically as a function of wavelength, similar to the scattering spectra measured from cell suspensions. The fitting parameters are listed in Table 1 for comparison with those for cell suspension. The trend in the results obtained for the cell culture agrees with those for the cell suspension.

Table 1. Fitting Parameters in the Unified Mie and Fractal Model

	Cell Suspension		Monolayer Cells
Measurement	Mie	Fractal	Fractal
Before acetic acid (AA)			
	$n_{Cell}=1.367$	$D_f=4.38$	$D_f=4.48$
		$\beta=12.77$	$\beta=18.54$
	$n_{Nucleus}=1.394$	$l_{max}=0.35$	$l_{max}=0.56$
After AA			
	$n'_{Cell}=1.360$	$D'_f=4.61$	$D'_f=4.77$
		$\beta'=23.08$	$\beta'=34.21$
	$n'_{Nucleus}=1.412$	$l'_{max}=0.27$	$l'_{max}=0.45$
$\Delta n_2/\Delta n_1$	—	1.81	1.85

In conclusion, the unified Mie and fractal model of cell light scattering provides an accurate interpretation of the scattering spectra measured from intact cells in suspension and culture. Quantitative information about cellular structural features and organization can be deduced from this unified model from wavelength- and angular-resolved light scattering spectroscopy. The fractal scattering from the fine subcellular structures is dominant at large scattering angles. This implies that the fractal scattering may contribute to degrading the image contrast in the optical imaging of cellular structures based on the backscattering measurement.

This study was supported by the Hong Kong Research Grants Council through grant HKUST6408/05M.

References

1. L. T. Perelman, V. Backman, M. Wallace, G. Zonios, R. Manoharan, A. Nusrat, S. Shields, M. Seiler, C. Lima, T. Hamano, I. Itzkan, J. Van Dam, J. M. Crawford, and M. S. Feld, Phys. Rev. Lett. **80**, 627 (1998).
2. K. Sokolov, R. Drezek, K. Gossage, and R. Richards-Kortum, Opt. Express **5**, 302 (1999).
3. A. Wax, C. Yang, V. Backman, K. Badizadegan, C. W. Boone, R. R. Dasari, and M. S. Feld, Biophys. J. **82**, 2256 (2002).
4. J. R. Mourant, T. M. Johnson, S. Carpenter, A. Guerra, T. Aida, and J. P. Freyer, J. Biomed. Opt. **7**, 378 (2002).
5. Z. Chen, A. Taflove, and V. Backman, Opt. Lett. **28**, 765 (2003).
6. X. Li, A. Taflove, and V. Backman, IEEE J. Sel. Top. Quantum Electron. **11**, 759 (2005).
7. R. S. Brock, X. H. Hu, D. A. Weidner, J. R. Mourant, and J. Q. Lu, J. Quant. Spectrosc. Radiat. Transf. **102**, 25 (2006).
8. M. Xu, T. T. Wu, and J. Y. Qu, Proc. SPIE **6446**, 64460Y (2007).
9. M. Moscoso, J. B. Keller, and G. Papanicolaou, J. Opt. Soc. Am. A **18**, 948 (2001).
10. M. Xu and R. R. Alfano, Opt. Lett. **30**, 3051 (2005).
11. M. C. Anderson, J. A. Jordan, A. R. Morse, and F. Sharp, *A Text and Atlas of Integrated Colposcopy: for Colposcopists, Histopathologists and Cytologists* (Chapman & Hall Medical, 1992).
12. T. T. Wu and J. Y. Qu, Appl. Opt. **46**, 4834 (2007).
13. W. J. Wiscombe, Appl. Opt. **19**, 1505 (1980).
14. A. Dunn, http://www.nmr.mgh.harvard.edu/~adunn/papers/dissertation/node73.html.
15. R. Lambert, J. F. Rey, and R. Sankaranarayanan, Endoscopy **35**, 437 (2003).